STRUCTURAL ROLE OF OSTEOCYTE LACUNAE ON MECHANICAL PROPERTIES OF BONE MATRIX: A COHESIVE FINITE ELEMENT STUDY

Wen Sang[1], Yihan Li[2], Jane Guignon[1], X. Sherry Liu[2], Ani Ural[1]

[1]Department of Mechanical Engineering, Villanova University,
800 Lancaster Avenue, Villanova, PA

[2]McKay Orthopaedic Research Laboratory, Department of Orthopaedic Surgery, Perelman School of Medicine, University of Pennsylvania, 332A Stemmler Hall, 36th Street and Hamilton Walk, Philadelphia, PA, USA

Full Length Article

Corresponding Author

Ani Ural
Associate Professor
Department of Mechanical Engineering
Villanova University
800 Lancaster Avenue, Villanova, PA 19085
E-mail: ani.ural@villanova.edu
Phone:(610) 519-7735
Fax: (610) 519-7312

ABSTRACT

Despite the extensive studies on biological function of osteocytes, there are limited studies that evaluated the structural role of osteocyte lacunae on local mechanical properties of the bone matrix. As a result, the goal of this study was to elucidate the independent contribution of osteocyte lacunae structure on mechanical properties and fracture behavior of the bone matrix uncoupled from its biological effects and bone tissue composition variation. This study combined cohesive finite element modeling with experimental data from a lactation rat model to evaluate the influence of osteocyte lacunar area porosity, density, size, axis ratio, and orientation on the elastic modulus, ultimate strength, and ultimate strain of the bone matrix as well as on local crack formation and propagation. It also performed a parametric study to isolate the influence of a single osteocyte lacunae structural property on the mechanical properties of the bone matrix. The experimental measurements demonstrated statistically significant differences in lacunar size between ovariectomized rats with lactation history and virgin groups (both ovariectomized and intact) and in axis ratio between rats with lactation history and virgins. There were no differences in mechanical properties between virgin and lactation groups as determined by the finite element simulations. However, there were statistically significant linear relationships between the physiological range of osteocyte lacunar area porosity, density, size, and orientation and the elastic modulus and ultimate strength of the bone matrix in virgin and lactation rats. The parametric study also revealed similar but stronger relationships between elastic modulus and ultimate strength and lacunar density, size, and orientation. The simulations also demonstrated that the osteocyte lacunae guided the crack propagation through local stress concentrations. In summary, this study enhanced the limited knowledge on the structural role of osteocyte lacunae on local mechanical properties of the bone matrix. These data are important in gaining a better understanding of the mechanical implications of the local modifications due to osteocytes in the bone matrix.

Keywords: *osteocyte lacunae, lactation, cohesive finite element modeling, bone mechanical properties, bone fracture*

1. INTRODUCTION

Osteocytes play an integral role in bone function as mechanosensory cells that respond to mechanical loading, participate in bone remodeling by regulating osteoblasts and osteoclasts, as well as engage in perilacunar/canalicular remodeling (PLR) (Qing et al., 2012). Osteocyte cell bodies are located in ellipsoidal spaces (~20x10x5 μm) called lacunae (Gauthier et al., 2018) and osteocyte cell processes extend from the lacunae in slender long channels (0.15-0.55 μm) called canaliculi (Varga et al., 2015).

Although biological function of osteocytes has been studied extensively, there are limited studies that evaluated the structural role of osteocyte lacunae on local mechanical properties of the bone matrix. Studies on osteocyte lacunar morphology and distribution have revealed structural changes in the osteocyte lacunae network with age, disease, and lactation. These studies showed that osteocyte lacunae density decreased with age (Ashique et al., 2017; Busse et al., 2010; Mori et al., 1997; Vashishth et al., 2000) and had significant inter-site differences (Busse et al., 2010; Carter et al., 2013b). Osteocyte density was also observed to be lower in bone from patients with fractures vs. healthy bone (Mullender et al., 2005; Qiu et al., 2003). Diseases such as osteopenia, osteopetrosis, and osteoarthritis influenced the osteocyte lacunae shape and area (van Hove et al., 2009). Bone from young donors (<50-year-old) demonstrated larger, flatter, and less spherical lacunae compared to old donors (>50-year-old) whereas the orientation of lacunae did not change (Carter et al., 2013a). In addition, osteocyte lacunae density was found to be lower in interstitial bone compared to osteonal bone (Qiu et al., 2005). Lactating mice or rats were found to have larger mean individual lacuna area and volume (Hemmatian et al., 2018; Kaya et al., 2017; Li et al., 2021; Qing et al., 2012) and lacunar porosity (Kaya et al., 2017) than controls whereas lacunae density, orientation, and sphericity were not different (Hemmatian et al., 2018). Furthermore, mineralized lacunae density increased with age (Busse et al., 2010) and with osteoporosis (Carpentier et al., 2012; Milovanovic et al., 2015). These findings indicate that the structural changes in osteocyte lacunae can potentially lead to local material property variation in the bone matrix independent of their biological effects.

Direct influence of osteocyte lacunae density and size on mechanical properties of bone was evaluated in only a couple of experimental studies. Osteocyte lacunae density was found to be the first or second best explanatory variable for elastic modulus in tension and compression as well as ultimate stress, yield stress, and pre-yield energy in compression in equine bone (Skedros et al., 2006). In a lactation mice model, the local elastic modulus decreased because of an increase in both the lacunar and canalicular volume fraction with no difference in bone matrix composition (Kaya et al., 2017). Theoretical calculations revealed small but statistically significant differences in apparent elastic modulus of the bone matrix due to variation in osteocyte lacunar size and density within the physiological range (Yeni et al., 2001). Finite element models also showed that existence of osteocyte lacunae lowered the apparent elastic modulus of the bone matrix (Hamed and Jasiuk, 2013). These observations suggest that the osteocyte lacunae structure influence mechanical properties of the bone matrix uncoupled from the material property variations in the tissue due to compositional changes.

Influence of osteocyte lacunae structure on crack initiation and propagation has been evaluated in a few studies. Experimental and computational studies identified osteocyte lacunae as strain/stress amplifiers (Ascenzi et al., 2013; Bonivtch et al., 2007; Nicolella et al., 2006; Varga et al., 2015; Verbruggen et al., 2012). One of the FE models showed that presence of lacunae increased local stress concentrations initiating failure of the tissue (Giner et al., 2014). Another FE model found that osteocyte lacuna size and orientation influenced the strains experienced by a lacuna (Kola et al., 2020). Diffuse damage locations under tensile loading were found to be associated with osteocyte lacunae (Reilly, 2000). Crack blunting by osteocyte lacunae was observed in ovine trabecular bone (Mullins et al., 2009). Osteocyte lacunae were shown to influence the orientation and direction of propagating cracks, however, microcracks initiated mainly at canals but not at osteocyte lacunae (Voide et al., 2009). These observations indicate that osteocyte lacunae network may have an influence on the local crack propagation behavior in the bone matrix.

In summary, the existing literature provides evidence of the structural modifications in osteocyte lacunae network and their influence on mechanical properties of bone. However, there is no systematic study that quantitatively delineate the contributions of osteocyte lacunae morphology, organization, and distribution to mechanical properties and fracture behavior of bone. This is partially due to the lack of experimental data that cover a wide spectrum of osteocyte lacunae morphology, distribution, and density. As a result, the objective of this study was to elucidate the independent contribution of osteocyte lacunae structure on mechanical properties and fracture behavior of bone uncoupled from its biological effects and bone tissue composition variation. Specifically, this study combined finite element (FE) modeling with experimental data from a lactation rat model to evaluate the influence of osteocyte lacunar area porosity, density, size, axis ratio, and orientation on the elastic modulus, ultimate strength, ultimate strain of the bone matrix and on local crack formation and propagation. In addition, it presented a parametric study to isolate the influence of a single osteocyte lacunae structural property on the mechanical properties of the bone matrix.

2. METHODS

2.1. Experimental assessment of lacunae morphology and distribution

Sixteen female Sprague Dawley rats were assigned to one of the two groups at the age of 3 months: Virgin and Lactation (n=8/group). Lactation rats underwent three repeated cycles of 3-week pregnancy, 3-week lactation, and 6-week post-weaning recovery. At the age of 12 months, both Virgin and Lactation rats were divided into non-OVX and OVX groups, and all rats in the OVX group underwent bilateral ovariectomy (OVX) surgery to simulate estrogen deficiency post-menopause. All groups of rats were euthanized at age 14-15 months (12 weeks post-OVX). Taken together, 4 groups of rats (n=4/group) were used in this study which were virgin non-ovariectomized (VnO), virgin ovariectomized (VO), lactation non-ovariectomized (LnO), and lactation ovariectomized (LO).

For all rats, right proximal tibiae were harvested immediately after euthanasia and processed for methyl methacrylate (MMA) embedding. A 3 mm thick sagittal bone segment of MMAembedded tibial diaphysis was cut by low-speed diamond saw, and the surface of the segment was manually polished in a wet condition with decreasing grain size until 0.06 μm of final polish and coated with carbon. Scanning electron microscope in backscatter mode (bSEM, Zeiss Supra 50VP) was applied to assess the structure of lacunae and canaliculi following a modification of the method described in previous studies (Kaya et al., 2017; Nango et al., 2016; Qing et al., 2012). Briefly, images of 1.5 mm-long segment of both medial and lateral tibial diaphysis located 2 mm below the proximal growth plate were acquired by bSEM at 15 kV accelerating voltage to measure the structure of lacunae (12 mm working distance, magnification of 300X with a resolution of 0.278 μm per pixel), and a customized MATLAB program was applied to threshold the bSEM images. ~500 lacunae were imaged for each sample to derive lacunar structural properties, including lacunar area porosity, density, size, axis ratio, and orientation. Lacunar area porosity was defined as the ratio of the total lacunar area (Tt.Lc.Ar) to the overall bone specimen area (B.Ar). Lacunar density was calculated as the total number of lacunae (Lc.N) divided by the overall bone specimen area (B.Ar). Lacunae size (Lc.S) represented the average area of an individual lacuna in each specimen. Axis ratio was defined as the ratio of the lacunar major axis to the minor axis. The orientation was calculated as the absolute value of the mean angle between major axes of lacunae and the horizontal (medial-lateral) axis in each specimen (which is perpendicular to the loading direction in the FE models described in Section 2.2).

2.2. Generation of FE models of bone specimens based on experimental measurements

Two-dimensional (2D) FE models of all specimens described in Section 2.1 were generated with dimensions ranging between 0.12-0.20 mm^2 representing the experimentally measured bone area. The models incorporated all experimentally identified lacunae as ellipses (Fig. 1a) based on the measured major and minor axis length, orientation, and centroidal coordinates. These data were imported into the finite element software, ABAQUS (version 6.18, Simulia, Providence, RI) using an in-house developed Python script that interfaces with a MATLAB (version R2019a, MathWorks, Natick, MA) code.

The models were meshed with linear triangular elements (Fig. 1b). The generated input files associated with all models were then processed with a previously developed MATLAB script (Mischinski and Ural, 2013) to insert zero-thickness cohesive interface elements (Fig. 1c, Fig. 2b) between the common edges of adjacent solid elements (Fig. 1b,c). This ensured that the cracks could initiate and propagate along the element boundaries without any prior assumption of crack initiation location or propagation trajectory. The models were fixed at the bottom edge and an incremental displacement loading (~ 2% overall strain) was applied at the top edge (Fig. 1b).

The solid plane strain elements in the models were assigned isotropic linear elastic properties including a Young's modulus of 20 GPa and a Poisson's ratio of 0.3 (Koester et al., 2008; Yeni et al., 2001). As in previous studies on bone (Demirtas et al., 2016; Ural and Vashishth, 2006), the cohesive model was defined by a bilinear traction-crack opening displacement relationship (Fig. 2a). The damage initiation is defined by the following interaction function (Camanho et al., 2003):

$$\left(\frac{t_n}{\sigma_{nc}}\right)^2 + \left(\frac{t_s}{\sigma_{sc}}\right)^2 = 1, \qquad (1)$$

where t_n and t_s are the current state of the normal and shear stresses and σ_{nc} and σ_{sc} are the critical normal and shear stresses. Damage evolution was defined by, G_c, the effective energy release rate, that represents the coupled normal and shear fracture energy. The cohesive model parameters (Table 1) were chosen based on the experimental data in the literature (Koester et al., 2008; Reilly and Burstein, 1975). The initial ascending slope of the cohesive model defined by δ_c is a penalty stiffness (Camanho et al., 2003). A compliance verification for the models was performed to select the initial ascending slope of the cohesive model. An initial slope of 10^9 N/mm^3 provided an elastic response that was within 2% of an equivalent solid model without any cohesive elements and still maintained numerical convergence.

In addition, mesh sensitivity studies were carried out to confirm that the results were not mesh dependent. The results demonstrated convergence between the two smallest mesh sizes (0.005 and 0.0025 mm global element edge size) investigated, including the elastic modulus (< 0.2% difference), ultimate strength (< 4% difference) and closely matching crack paths. As a result, mesh size of 0.0025 was chosen. The number of solid elements in the models ranged from 75,017 to 93,649, and the number of cohesive elements ranged from 112,015 to 139,856 as a result of varying model sizes.

In order to further investigate the interactions between lacunae and crack propagation, as well as the influence of mineralized lacunae, four modified models were generated by filling up a subset of the original lacunae with solid material in one of the models from group VnO. To test the influence of distribution of mineralized lacunae on the crack path, the mineralized lacunae were placed either in a clustered (Fig. 11b) or scattered (Fig. 11c) form in the models. A higher elastic modulus, 23 GPa, than the surrounding bone was assigned to mineralized lacunae to represent the higher mineral content in these regions (Busse et al., 2009; Rho et al., 2002) with the assumption that mineralized lacunae were fully calcified and filled with the mineral phase.

2.3. Generation of FE Models for Parametric study

In the experimentally evaluated rat bone specimens, variation in all osteocyte lacunae structural parameters occur simultaneously which may confound the direct influence of a single structural parameter on bone matrix mechanical properties. As a result, a parametric study was performed to further elucidate the relationship between individual lacunar structural parameters and bone matrix mechanical properties.

Four groups of models were generated for the parametric study. In each group, one of the four structural parameters (lacunae density, lacunae size, lacunae orientation, and lacunae axis ratio) was varied while the remaining three parameters were held constant. Since lacunar area porosity is dependent on the lacunae density and size, it was not included in the independent variables that were varied. Seven different cases were investigated for each parameter including: (i) mean value of all the individual bone samples from all rat groups (ii-iii) one standard deviation up and down the mean value, (iv-v) two standard deviations up and down the mean value, (vi-vii) minimum and maximum values that were observed in the bone samples. The other three parameters that were held constant were assigned their pooled mean values from all rat groups. Detailed list of the parametric simulations and the values used for each parameter can be found in Table S1.

To perform the parametric study, another MATLAB script was developed to generate FE models of osteocyte lacunae with the selected structural parameter values that were randomly placed in the bone area. Following the generation of the osteocyte lacunae network, the same material properties, boundary conditions, and analysis procedures were applied as in the models based on experimental measurements described in Section 2.2.

2.4. Data extraction and processing

A total of 132 simulations using models based on experimental measurements (32 simulations per group plus 4 simulations on mineralized lacunar models) were run to evaluate how the local mechanical properties of bone were influenced by the lacunae structure and distribution. An additional 28 simulations were run for the parametric study where one of the structural parameters was varied while other parameters were held constant. The load-displacement data were extracted to plot the stress-strain curve for each model representing the average stress on the loading surface (total load/top edge length with unit thickness), and the average strain (total displacement/original height of the model). The elastic modulus and ultimate strengths were extracted from the stress-strain curve. The damage energy was calculated as the total energy dissipated for damage and crack formation at the cohesive interface elements at a strain of 1.5% where the stress is greatly reduced compared to the maximum stress and the variation of stress is lower than 2%. The variation of elastic modulus, ultimate strength, ultimate strain and damage energy with the lacunar area porosity, density, size, axis ratio, and orientation were evaluated using linear regression. Mechanical and structural property comparison between rat groups was performed via one-way analysis of variance (ANOVA) test, post-hoc Tukey, using IBM SPSS Statistics (version 25, IBM

Corp.). In addition, crack paths were extracted from the models to assess the interaction of crack propagation with lacunae.

3. RESULTS

3.1. Groupwise comparison of structural parameters of lacunae

Groupwise structural parameters of lacunae are shown in Figure 3, where each data point represents the average value of eight samples from the same animal. The mean values of structural properties for each group are listed in Table 2. Groupwise comparison of the structural parameters including lacunar area porosity, density, axis ratio, size, and orientation using one-way ANOVA showed that statistically significant differences only existed in lacunar size between LO and virgin groups (LO *vs.* VnO, $p = 0.035$; LO *vs.* VO, $p = 0.021$) (Fig. 3c) as well as in axis ratio between lactation groups and virgin groups ($p < 0.01$) (Fig. 3e). Other structural parameters did not show significant differences among groups.

3.2. Groupwise comparison of mechanical properties of bone incorporating lacunae

Stress-strain curves of four representative models (one from each group) are shown in Figure 4. All mechanical properties are determined based on the stress-strain curves obtained from the simulations.

Groupwise mechanical property data are shown in Figure 5, where each data point represents the average value of eight models associated with the specimens from the same animal. The mean values of mechanical properties for each group are listed in Table 3. No statistically significant differences were observed in the mechanical properties among the groups based on one-way

ANOVA.

3.3. Variation of mechanical properties with structural parameters of lacunae in rat bone specimens

To understand the relationship between elastic properties of bone and the structural parameters of lacunae, the variation of elastic moduli of all the models with respect to each of the four structural parameters were plotted (Fig. 6). Elastic modulus decreased linearly with lacunar area porosity, density, and size (Fig. 6a, b, c), with a stronger relationship with lacunar area porosity (Fig. 6a, Table 4). Elastic modulus showed a weak positive linear variation with orientation (Fig. 6d, Table 4). As the orientation angle increased, where the major axes of most lacunae were oriented in the same direction as the loading, the models exhibited slightly higher elastic modulus. No statistically significant relationship between elastic modulus and axis ratio was observed (Fig. 6e).

Ultimate strength also decreased linearly with both lacunar area porosity, density and size (Fig. 7a, b, c), with a stronger relationship with lacunar area porosity (Fig. 7a, Table 4). Ultimate strength showed a positive linear variation with orientation (Fig. 7d, Table 4). As the orientation angle increased, where most lacunae were oriented in the same direction as the loading, the models exhibited higher ultimate strength. Compared with elastic modulus, ultimate strength showed stronger correlations with the structural parameters of lacunae (Table 4). Similar to elastic modulus, no statistically significant relationship between ultimate strength and axis ratio was observed (Fig. 7e).

Ultimate strain showed very weak but statistically significant linear dependence on lacunae area porosity, density, and orientation (Fig. S2). Damage energy did not demonstrate statistically significant correlations with any of the structural parameters of lacunae (Fig. S3).

3.4. Variation of mechanical properties with structural parameters in parametric models

The parametric study showed similar relationships as found in the models based on experimental measurements (Section 3.3) with stronger trends. Elastic modulus was found to linearly decrease with increasing lacunar density and size (Fig. 8a, b) and linearly increase with increasing lacunae orientation angle that aligned the major axis of the lacunae with the loading direction ($R^2 > 0.98$, $p < 0.001$) (Fig. 8c). Elastic modulus also decreased with increasing axis ratio (R^2=0.89, $p = 0.002$) (Fig. 8d) which was not observed in the models based on rat bone specimens. Ultimate strength decreased with lacunar density ($R^2 = 0.74$, $p = 0.013$), size ($R^2 = 0.92$, $p < 0.001$) and increased with increasing lacunae orientation angle that aligned the major axis of the lacunae with the loading direction ($R^2 = 0.87$, $p = 0.002$) (Fig. 9a, b and c) with no statistically significant dependence on axis ratio (Fig. 9d).

Additionally, different from the models based on experimental measurements, parametric models showed strong linear relationships between ultimate strain and lacunar size ($R^2 = 0.79$, $p = 0.007$) and lacunae orientation angle ($R^2 = 0.73$, $p = 0.015$) (Fig. S3). Damage energy still did not show any statistically significant correlations to the lacunar parameters (Fig. S4).

3.5. Interaction of crack initiation and propagation with osteocyte lacunae

Crack initiation occurred at local stress concentrations around the lacunae (Fig. 10) which were larger along the axis perpendicular to the loading axis. As the load increased, minor cracks close to the surface of the lacunae formed (Fig. 11a, Stage 2). Further increase in the loading resulted in the merging of these minor cracks which transitioned into a major crack. The major crack continued to propagate while stress concentrations at other parts of the model were released (Fig. 11a, Stages 3-5). During this process, uncracked ligament bridges formed between adjacent lacunae that were in the path of the major crack (Fig. 12).

The interaction of the crack path with lacunae was further investigated by comparing the process of crack formation in one of the original models to that in modified models with mineralized lacunae (Fig. 11b, c). The results of these simulations revealed that if mineralized lacunae occurred in the vicinity of the original crack path (Fig. 11a), the major crack would then find another path to get through the mineralized region while maintaining the rest of the path unchanged (Fig. 11b). If the mineralized lacunae occurred further away from the original crack path (Fig. 11c) then the major crack remained almost the same as that in the original model.

4. DISCUSSION

This study presented a new computational model integrated with experimental measurements that has the capability to quantify the independent contribution of osteocyte lacunae structure on mechanical properties and fracture behavior of the bone matrix. The use of finite element modeling enabled decoupling the role of osteocyte lacunae structure on mechanical properties of the bone matrix uncoupled from its biological effects and the bone tissue composition variation. The results of this study not only improved the understanding of how modifications in osteocyte lacunae structure during lactation influences local mechanical properties of the bone matrix but also provided a widely applicable modeling approach to assess the changes in mechanical properties of the bone matrix due to variation in osteocyte lacunae structure caused by other changes such as aging or disease.

The experimental measurements revealed significantly greater lacunar size in ovariectomized rats with lactation history than both ovariectomized and intact virgin rats. Moreover, for both ovariectomized and intact rats, lactation history resulted in elongated lacunae as compared to virgins. Previous studies has reported that osteocytic PLR led to greater lacunar size in lactating animals *vs.* virgins (Kaya et al., 2017; Li et al., 2021; Qing et al., 2012). However, osteocytes begin to deposit minerals on the perilacunar/canalicular surfaces after weaning, resulting in comparable size of lacunae between post-weaning *vs.* virgin animals (Kaya et al., 2017; Li et al., 2021; Qing et al., 2012). Our results indicated that multiple cycles of reproduction and lactation may lead to significant alterations in lacunar morphology, as indicated by increased aspect ratio of lacunae. Moreover, another investigation from our research group demonstrated that estrogen deficiency would trigger osteocyte PLR in rats with histories of multiple cycles of reproduction and lactation, resulting in enlarged lacunae (Li et al., 2018).

The mechanical properties including elastic modulus, ultimate strength, ultimate strain, and dissipated damage energy were very close among the rat groups and were not statistically different. This may be due to the limited difference in lacunar structural parameters between lactation and virgin groups. Axis ratio, one of the statistically different parameters among the groups did not show any relation to the mechanical properties. Lacunae size was statistically different between LO group and virgin groups. The mechanical properties demonstrated the strongest relationship with lacunae area porosity, therefore, axis ratio and lacunae size may not have a strong enough influence to result in statistically significant differences in the mechanical properties among groups. These results may indicate that in the absence of compositional modifications in the bone matrix the structural changes in osteocyte lacunae alone due to lactation may not reduce the local mechanical properties compared to virgin rats. Although, there were no differences in mechanical properties of the bone matrix among groups due to changes in osteocyte lacunae structure, the statistically different differences in lacunar axis ratio and size between lactation and virgin groups can potentially impact the stress/strain microenvironment of the osteocytes. This may directly influence mechanosensory responses of the cells and their impact on mechanical integrity of the bone matrix during lactation.

The results showed a statistically significant linear relationship between the physiological range of osteocyte lacunar area porosity, density, size, and orientation and the elastic modulus and ultimate strength of the bone matrix in virgin and lactation rats. An increase in the lacunar area porosity, density, and size reduced the elastic modulus and the ultimate strength of the bone matrix with the strongest impact coming from lacunar area porosity. These results are in line with the reduced elastic modulus with increasing lacunar area porosity and size measured experimentally (Kaya et al., 2017) and estimated theoretically (Yeni et al., 2001). The results also showed that as more lacunae had their major axes oriented away from the loading direction, the mechanical properties of the bone matrix, particularly ultimate strength, were reduced. This was due to the increase in stress concentrations that were formed around the lacunae as the major axis of the lacunae deviated away from the loading direction enhancing crack formation and propagation (Fig. 10b, c). The variations in elastic modulus and ultimate strength with respect to the osteocyte structural parameters although statistically significant, were in a narrow range (within 2% for elastic modulus and within 8% for ultimate strength based on the linear fit equations over the physiological range of all structural parameters). This indicates that in normal and lactation rat bone the mechanical property variation within the physiological range of osteocyte lacunae structure may be limited but detectable. Furthermore, these results show that it may be possible to detect differences in mechanical properties of the bone matrix as a result of observed variation in osteocyte lacunae structure due to aging, disease, or fracture (Ashique et al., 2017; Busse et al., 2010; Carter et al., 2013a; Mori et al., 1997; Mullender et al., 2005; Qiu et al., 2003; van Hove et al., 2009; Vashishth et al., 2000). In this study, there was no relationship between the energy dissipated during damage and crack formation, a measure of fracture resistance, and the osteocyte lacunae structural parameters. This indicates that although the local elastic modulus and ultimate strength were affected from the osteocyte lacunae structural changes in the physiological range, the modifications did not influence the fracture resistance of the bone matrix.

In addition to assessing the relationship between osteocyte lacunae structural parameters and bone matrix mechanical properties in rat bone specimens, a parametric study was performed to isolate the influence of a single osteocyte lacunae structural parameter on bone matrix mechanical properties. These groups of simulations demonstrated similar but stronger relationships between elastic modulus and ultimate strength and lacunar density, size, and orientation. Additional relationships between elastic modulus and axis ratio as well as between ultimate strain and lacunar size were also determined. The stronger and additional relationships observed in the parametric study compared to that observed in the FE models based on rat bone specimens is due to the confounding effects that come from the simultaneous variation of each structural parameter in rat bone specimens. When the structural parameters vary concurrently, they may affect the mechanical properties in opposing directions resulting in a cumulative effect that may not reveal the direct influence of a single structural parameter on the mechanical properties. As a result, the parametric study performed in this study provided important insights about the direct relationship between mechanical properties and each osteocyte lacunae structural property.

This study also evaluated the interaction of osteocyte lacunae and crack formation and propagation. The simulation results showed that osteocyte lacunae act as stress concentrators as shown in previous studies (Ascenzi et al., 2013; Bonivtch et al., 2007; Nicolella et al., 2006; Varga et al., 2015; Verbruggen et al., 2012). This leads to crack formation near their boundaries in line with experimental observations that reported an association between diffuse damage formation and osteocyte lacunae under tensile loading (Reilly, 2000). The models in the current study only incorporated osteocyte lacunae and did not include the influence of larger length scale features such as osteons on crack formation. A previous experimental study reported that microcracks initiated mainly at canals and while propagating went through osteocyte lacunae which influenced the crack orientation and direction (Voide et al., 2009). In the simulations, osteocyte lacunae demonstrated a guiding effect on the cracks i.e. attracted a nearby crack due to stress concentrations near lacunar boundaries. This behavior was most apparent in the simulations with the mineralized lacunae models. In these models, the filled mineralized lacunae no longer attracted the crack. As a result, the crack path was altered locally passing through other normal lacunae while the rest of the original crack path further away from the mineralized lacunae remained unchanged. This outcome suggests that osteocyte lacunae can guide the crack propagation through local stress concentrations which agrees with experimental observations (Voide et al., 2009). In the simulations, osteocyte lacunae also resulted in the formation of uncracked ligament bridges between closely located lacunae which may contribute to fracture toughening during crack propagation.

This study presented the first use of cohesive finite element modeling in representing the mechanical influence of osteocyte lacunar structure and assessing the interaction of osteocyte lacunae with crack formation and propagation. The use of finite element modeling made it possible to decouple the structural role of osteocyte lacunae from its biological effects and assess the contribution of the structural variation in osteocyte lacunae on the mechanical properties of the bone matrix independent of bone composition. Despite these important strengths, the current study has several limitations. One of the limitations is that it did not incorporate any material property variation in the bone matrix and only evaluated the influence of osteocyte lacunae structure on the mechanical properties of the bone matrix. Previous studies did not observe bone compositional differences between lactation and virgin mice suggesting that the structural changes in the osteocyte lacunae caused the measured reduction in local elastic modulus (Kaya et al., 2017). This supports our approach in this study. In the potential presence of modification in local bone composition with lactation, the local bone matrix mechanical properties would be determined by the cumulative influence of osteocyte lacunae structure and bone composition. Bone compositional information can easily be incorporated in the current model if a corresponding local map of mechanical properties is available. Another limitation is that the models did not incorporate any preexisting microcracks. Several studies in the literature showed an increase in microdamage with a reduction in osteocyte density in human bone (Qiu et al., 2005; Vashishth et al., 2000). This indicates that although a reduction in the osteocyte lacunar density may increase the local elastic modulus and ultimate strength, it may over time impair remodeling and microcrack detection/repair resulting in reduced fracture resistance. The models only incorporated osteocyte lacunae but not canaliculi emanating from the lacunae. The main reason for this is that in 2D models a network of canaliculi would lead to an underrepresentation of the real 3D bone matrix distribution which can result in unrealistically low apparent mechanical properties for the bone matrix. The potential changes in the canaliculi size and area due to lactation can be incorporated in future extensions of this modeling approach to 3D.

In summary, this study systematically quantified how mechanical properties and fracture behavior of the bone matrix vary due to changes in osteocyte lacunae morphology and distribution using a lactation rat model. It also presented a parametric study that isolated the influence of a single osteocyte lacunae structural property on bone matrix mechanical properties. The results enhanced the limited knowledge on the structural role of osteocyte lacunae on local mechanical properties of the bone matrix. The outcomes elucidated the independent contribution of osteocyte lacunae structure on mechanical properties and fracture behavior of the bone matrix uncoupled from its biological effects and bone tissue composition variation. In addition, they provided insights into the local changes in the osteocyte lacunae structure and mechanical properties of the bone matrix due to lactation history. The FE model that is developed in this study can further be extended to assess the influence of variation in osteocyte lacunae structure on the mechanical properties of the bone matrix due to other causes such as aging, disease, or fracture status in human bone. These data are important in gaining a better understanding of the mechanical implications of the local modifications due to osteocytes in the bone matrix.

ACKNOWLEDGEMENTS

This study was partially supported by National Institute of Health NIH/NIAMS R01-AR071718 and National Science Foundation (NSF) Award #1653216.

REFERENCES

Ascenzi, M.-G., Kawas, N.P., Lutz, A., Kardas, D., Nackenhorst, U., Keyak, J.H., 2013. Individual-specific multi-scale finite element simulation of cortical bone of human proximal femur. Journal of Computational Physics 244, 298-311.

Ashique, A.M., Hart, L.S., Thomas, C.D.L., Clement, J.G., Pivonka, P., Carter, Y., Mousseau, D.D., Cooper, D.M.L., 2017. Lacunar-canalicular network in femoral cortical bone is reduced in aged women and is predominantly due to a loss of canalicular porosity. Bone Reports 7, 9-16.

Bonivtch, A.R., Bonewald, L.F., Nicolella, D.P., 2007. Tissue strain amplification at the osteocyte lacuna: a microstructural finite element analysis. Journal of biomechanics 40, 2199-2206.

Busse, B., Djonic, D., Milovanovic, P., Hahn, M., Püschel, K., Ritchie, R.O., Djuric, M., Amling, M., 2010. Decrease in the osteocyte lacunar density accompanied by hypermineralized lacunar occlusion reveals failure and delay of remodeling in aged human bone. Aging Cell 9, 1065-1075.

Busse, B., Hahn, M., Soltau, M., Zustin, J., Püschel, K., Duda, G.N., Amling, M., 2009. Increased calcium content and inhomogeneity of mineralization render bone toughness in osteoporosis: mineralization, morphology and biomechanics of human single trabeculae. Bone 45, 1034-1043.

Camanho, P.P., Davila, C.G., de Moura, M.F., 2003. Numerical Simulation of Mixed-Mode Progressive Delamination in Composite Materials. Journal of Composite Materials 37, 1415-1438.

Carpentier, V.T., Wong, J., Yeap, Y., Gan, C., Sutton-Smith, P., Badiei, A., Fazzalari, N.L., Kuliwaba, J.S., 2012. Increased proportion of hypermineralized osteocyte lacunae in osteoporotic and osteoarthritic human trabecular bone: Implications for bone remodeling. Bone 50, 688-694.

Carter, Y., Thomas, C.D.L., Clement, J.G., Cooper, D.M.L., 2013a. Femoral osteocyte lacunar density, volume and morphology in women across the lifespan. Journal of Structural Biology 183, 519-526.

Carter, Y., Thomas, C.D.L., Clement, J.G., Peele, A.G., Hannah, K., Cooper, D.M.L., 2013b. Variation in osteocyte lacunar morphology and density in the human femur — a synchrotron radiation micro-CT study. Bone 52, 126-132.

Demirtas, A., Curran, E., Ural, A., 2016. Assessment of the effect of reduced compositional heterogeneity on fracture resistance of human cortical bone using finite element modeling. Bone 91, 92-101.

Gauthier, R., Langer, M., Follet, H., Olivier, C., Gouttenoire, P.-J., Helfen, L., Rongiéras, F., Mitton, D., Peyrin, F., 2018. 3D micro structural analysis of human cortical bone in paired femoral diaphysis, femoral neck and radial diaphysis. Journal of Structural Biology 204, 182-190.

Giner, E., Arango, C., Vercher, A., Javier Fuenmayor, F., 2014. Numerical modelling of the mechanical behaviour of an osteon with microcracks. Journal of the Mechanical Behavior of

Biomedical Materials 37, 109-124.

Hamed, E., Jasiuk, I., 2013. Multiscale damage and strength of lamellar bone modeled by cohesive finite elements. Journal of the mechanical behavior of Biomedical Materials 28, 94-110.

Hemmatian, H., Jalali, R., Semeins, C.M., Hogervorst, J.M.A., van Lenthe, G.H., Klein-Nulend, J., Bakker, A.D., 2018. Mechanical Loading Differentially Affects Osteocytes in Fibulae from Lactating Mice Compared to Osteocytes in Virgin Mice: Possible Role for Lacuna Size. Calcified Tissue International 103, 675-685.

Kaya, S., Basta-Pljakic, J., Seref-Ferlengez, Z., Majeska, R.J., Cardoso, L., Bromage, T.G., Zhang, Q., Flach, C.R., Mendelsohn, R., Yakar, S., 2017. Lactation-Induced Changes in the Volume of Osteocyte Lacunar-Canalicular Space Alter Mechanical Properties in Cortical Bone Tissue. Journal of Bone and Mineral Research 32, 688-697.

Koester, K.J., Ager, J., Ritchie, R., 2008. The true toughness of human cortical bone measured with realistically short cracks. Nature Materials 7, 672-677.

Kola, S.K., Begonia, M.T., Tiede-Lewis, L.M., Laughrey, L.E., Dallas, S.L., Johnson, M.L., Ganesh, T., 2020. Osteocyte lacunar strain determination using multiscale finite element analysis. Bone Reports 12, 100277.

Li, Y., De Bakker, C., Tseng, W.-J., Zhao, H., Parajuli, A., Wang, L., Liu, X.S., 2018. Peri-lacunar/canalicular (PLC) remodeling enhances mechano-sensitivity in rat maternal bone when subjected to estrogen deficiency, Journal of Bone and Mineral Research 33, pp. 35-35.

Li, Y., de Bakker, C.M., Lai, X., Zhao, H., Parajuli, A., Tseng, W.-J., Pei, S., Meng, T., Chung, R., Wang, L., 2021. Maternal bone adaptation to mechanical loading during pregnancy, lactation, and post-weaning recovery. Bone, 116031.

Milovanovic, P., Zimmermann, E.A., Riedel, C., vom Scheidt, A., Herzog, L., Krause, M., Djonic, D., Djuric, M., Püschel, K., Amling, M., 2015. Multi-level characterization of human femoral cortices and their underlying osteocyte network reveal trends in quality of young, aged, osteoporotic and antiresorptive-treated bone. Biomaterials 45, 46-55.

Mischinski, S., Ural, A., 2013. Interaction of microstructure and microcrack growth in cortical bone: a finite element study. Computer Methods in Biomechanics and Biomedical Engineering 16, 81-94.

Mori, S., Harruff, R., Ambrosius, W., Burr, D.B., 1997. Trabecular bone volume and microdamage accumulation in the femoral heads of women with and without femoral neck fractures. Bone 21, 521-526.

Mullender, M.G., Tan, S.D., Vico, L., Alexandre, C., Klein-Nulend, J., 2005. Differences in Osteocyte Density and Bone Histomorphometry Between Men and Women and Between Healthy and Osteoporotic Subjects. Calcified Tissue International 77, 291-296.

Mullins, L., Sassi, V., McHugh, P., Bruzzi, M., 2009. Differences in the crack resistance of interstitial, osteonal and trabecular bone tissue. Annals of biomedical engineering 37, 2574.

Nango, N., Kubota, S., Hasegawa, T., Yashiro, W., Momose, A., Matsuo, K., 2016. Osteocyte-directed bone demineralization along canaliculi. Bone 84, 279-288.

Nicolella, D.P., Moravits, D.E., Gale, A.M., Bonewald, L.F., Lankford, J., 2006. Osteocyte lacunae tissue strain in cortical bone. Journal of biomechanics 39, 1735-1743.

Qing, H., Ardeshirpour, L., Divieti Pajevic, P., Dusevich, V., Jähn, K., Kato, S., Wysolmerski, J., Bonewald, L.F., 2012. Demonstration of osteocytic perilacunar/canalicular remodeling in mice during lactation. Journal of Bone and Mineral Research 27, 1018-1029.

Qiu, S., Rao, D.S., Palnitkar, S., Parfitt, A.M., 2003. Reduced Iliac Cancellous Osteocyte Density in Patients With Osteoporotic Vertebral Fracture. Journal of Bone and Mineral Research 18, 1657-1663.

Qiu, S., Sudhaker Rao, D., Fyhrie, D.P., Palnitkar, S., Parfitt, A.M., 2005. The morphological association between microcracks and osteocyte lacunae in human cortical bone. Bone 37, 10-15.

Reilly, D.T., Burstein, A.H., 1975. The elastic and ultimate properties of compact bone tissue. Journal of Biomechanics 8, 393-405.

Reilly, G.C., 2000. Observations of microdamage around osteocyte lacunae in bone. Journal of Biomechanics 33, 1131-1134.

Rho, J.Y., Zioupos, P., Currey, J.D., Pharr, G.M., 2002. Microstructural elasticity and regional heterogeneity in human femoral bone of various ages examined by nano-indentation. Journal of Biomechanics 35, 189-198.

Skedros, J.G., Dayton, M.R., Sybrowsky, C.L., Bloebaum, R.D., Bachus, K.N., 2006. The influence of collagen fiber orientation and other histocompositional characteristics on the mechanical properties of equine cortical bone. Journal of Experimental Biology 209, 3025-3042.

Ural, A., Vashishth, D., 2006. Cohesive finite element modeling of age-related toughness loss in human cortical bone. Journal of Biomechanics 39, 2974-2982.

van Hove, R.P., Nolte, P.A., Vatsa, A., Semeins, C.M., Salmon, P.L., Smit, T.H., Klein-Nulend, J., 2009. Osteocyte morphology in human tibiae of different bone pathologies with different bone mineral density — Is there a role for mechanosensing? Bone 45, 321-329.

Varga, P., Hesse, B., Langer, M., Schrof, S., Männicke, N., Suhonen, H., Pacureanu, A., Pahr, D., Peyrin, F., Raum, K., 2015. Synchrotron X-ray phase nano-tomography-based analysis of the lacunar–canalicular network morphology and its relation to the strains experienced by osteocytes in situ as predicted by case-specific finite element analysis. Biomechanics and Modeling in Mechanobiology 14, 267-282.

Vashishth, D., Verborgt, O., Divine, G., Schaffler, M.B., Fyhrie, D.P., 2000. Decline in osteocyte lacunar density in human cortical bone is associated with accumulation of microcracks with age. Bone 26, 375-380.

Verbruggen, S.W., Vaughan, T.J., McNamara, L.M., 2012. Strain amplification in bone mechanobiology: a computational investigation of the <i>in vivo</i> mechanics of osteocytes. Journal of The Royal Society Interface 9, 2735-2744.

Voide, R., Schneider, P., Stauber, M., Wyss, P., Stampanoni, M., Sennhauser, U., van Lenthe, G.H.,

Müller, R., 2009. Time-lapsed assessment of microcrack initiation and propagation in murine cortical bone at submicrometer resolution. Bone 45, 164-173.
Yeni, Y.N., Vashishth, D., Fyhrie, D.P., 2001. Estimation of bone matrix apparent stiffness variation caused by osteocyte lacunar size and density. Journal of biomechanical engineering 123, 10-17.

TABLES

Table 1. Cohesive model parameters including critical normal and shear stress as well as effective fracture energy based on experimental data reported in the literature (Koester et al., 2008; Reilly and Burstein, 1975).

Cohesive Properties	
σ_{nc}	53 MPa
σ_{sc}	68 MPa
G_c	0.05 N/mm

Table 2: Average values and standard deviations of structural parameters of osteocyte lacunae for each rat group.

	Tt.Lc.Ar/B.Ar (%)	Lc.N/B.Ar (#/mm^2)	Lc.S (mm^2)	Orientation (degree)	Axis Ratio
VnO	0.87±0.19	315.6±35.6	26.9±2.8	64.4±5.2	2.36±0.07
VO	0.85±0.14	307.1±22.9	26.6±2.6	63.8±6.1	2.44±0.07
LnO	0.78±0.14	261.5±38.8	28.8±2.7	63.2±13.2	3.05±0.17
LO	0.90±0.20	293.8±25.6	29.6±3.5	63.2±6.9	3.12±0.23

Table 3: Average values and standard deviations of mechanical properties derived from FE models for each rat group.

	Ultimate Strain (%)	Ultimate Strength (MPa)	Elastic Modulus (MPa)	Damage Energy (mJ)
VnO	0.286±0.005	56.5±1.1	22,378±246	0.039±0.008
VO	0.285±0.006	56.3±1.2	22,506±231	0.041±0.010
LnO	0.285±0.005	56.3±1.3	22,460±216	0.044±0.007
LO	0.285±0.006	55.6±1.2	22,329±219	0.038±0.008

Table 4: Linear regression equations between mechanical properties derived from FE models and structural parameters of osteocyte lacunae (Units are as in Figs. 6 and 7).

Mechanical Property	Structural Parameter	Linear Correlation Slope	Intercept	R^2	*p* value
Elastic Modulus	Tt.Lc.Ar/B.Ar	-53.36×10^3	22.87×10^3	0.36	<0.001
	Lc.N/B.Ar	-1.13	22.75×10^3	0.17	<0.001
	Lc.S	-18.29	22.94×10^3	0.14	<0.001
	Orientation	6.44	22.00×10^3	0.06	0.005
Ultimate Strength	Tt.Lc.Ar/B.Ar	-498.11	60.43	0.41	<0.001
	Lc.N/B.Ar	-11.67×10^{-3}	59.66	0.23	<0.001
	Lc.S	-0.15	60.57	0.13	<0.001
	Orientation	119.71×10^{-3}	48.51	0.29	<0.001

FIGURES

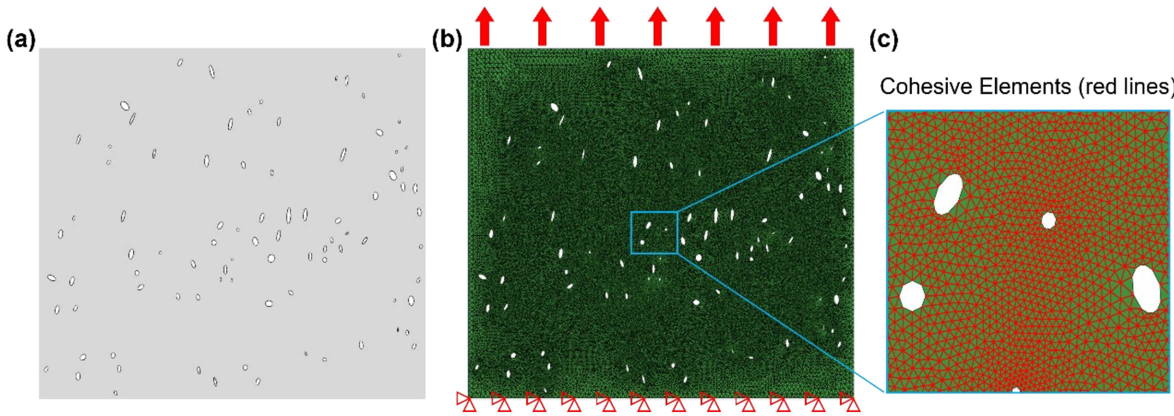

Figure 1: A sample FE model of osteocyte lacunae network from VnO group based on experimental measurements. (b) FE mesh of model in (a) showing the loading and boundary conditions. (c) Close-up view of FE model highlighting the inserted cohesive elements (marked as red lines) lying in between the coincident elemental edges.

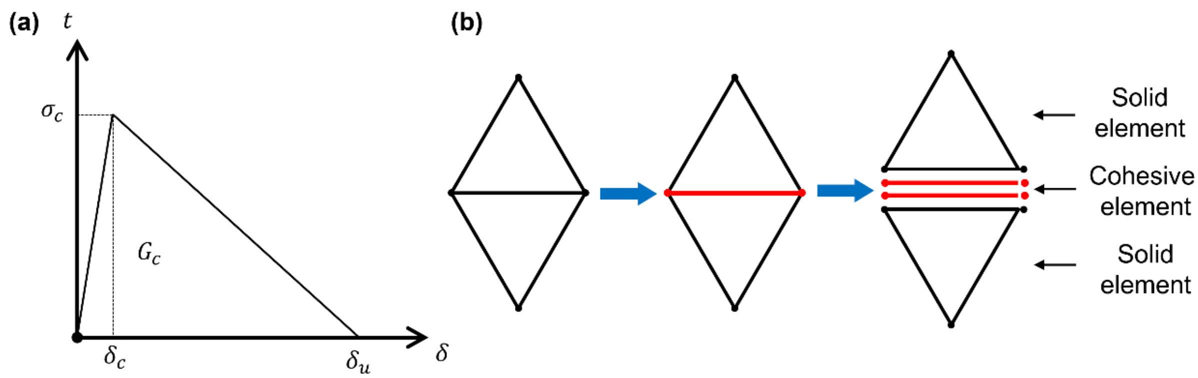

Figure 2: (a) Traction-displacement relationship defining the cohesive zone model. (b) 2D triangular solid elements and the compatible 2D cohesive element with four nodes showing the initial zero-thickness configuration.

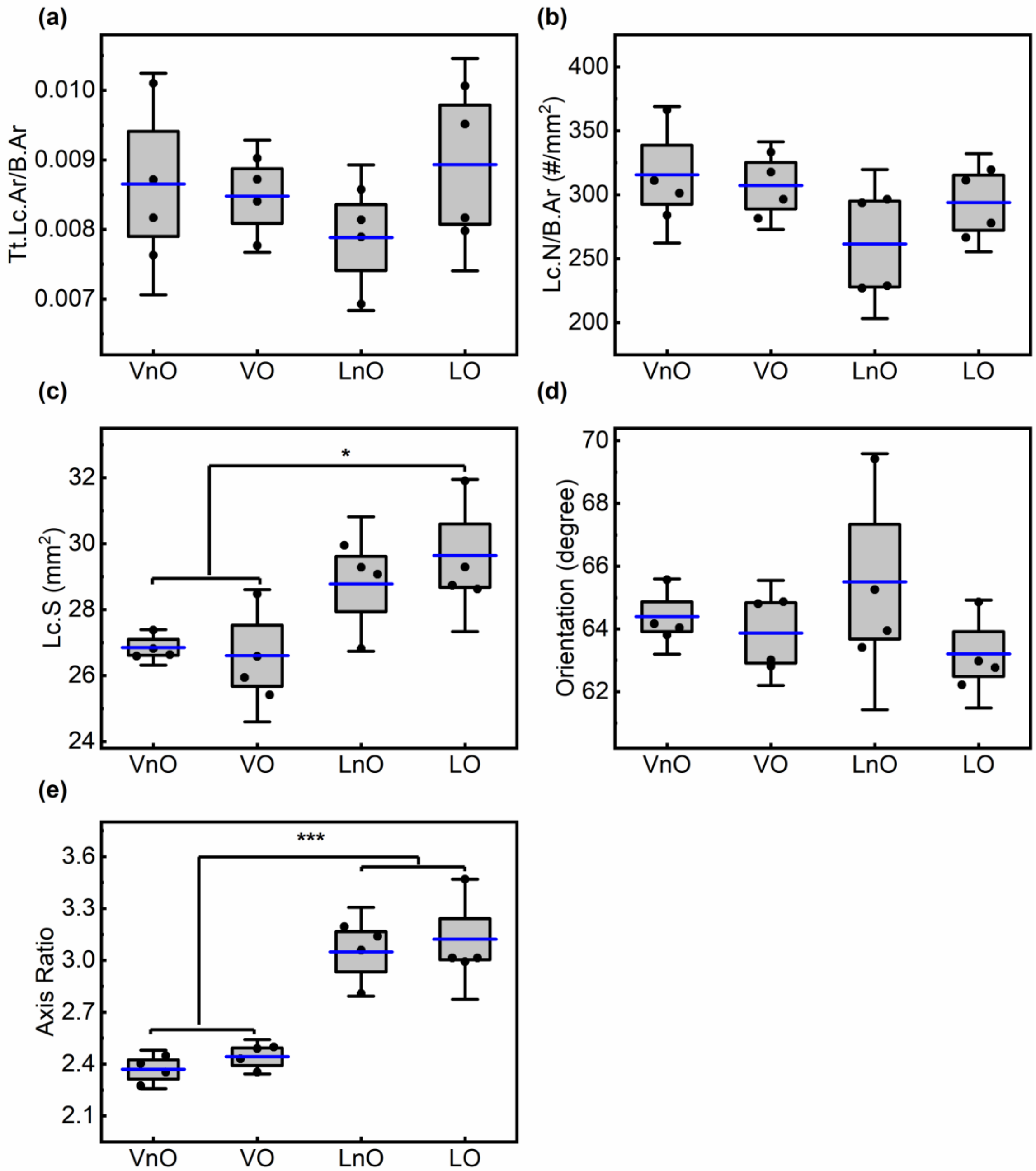

Figure 3: Groupwise comparison of experimentally measured structural parameters of osteocyte lacunae: (a) area porosity, (b) density, (c) size, (d) orientation, and (e) axis ratio. Error bars represent 1.5 times the standard deviation. Blue lines mark the mean values. Note that stars indicate statistically significant differences between the corresponding groups (*$p < 0.05$, ***$p < 0.01$).

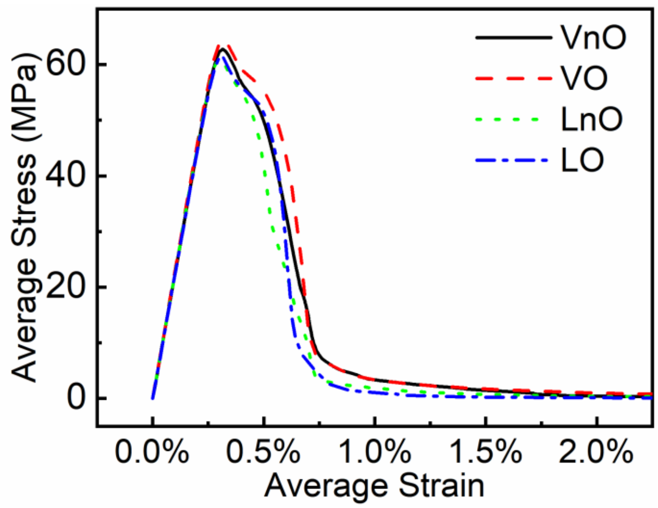

Figure 4: Stress-strain curves of four representative models from each group.

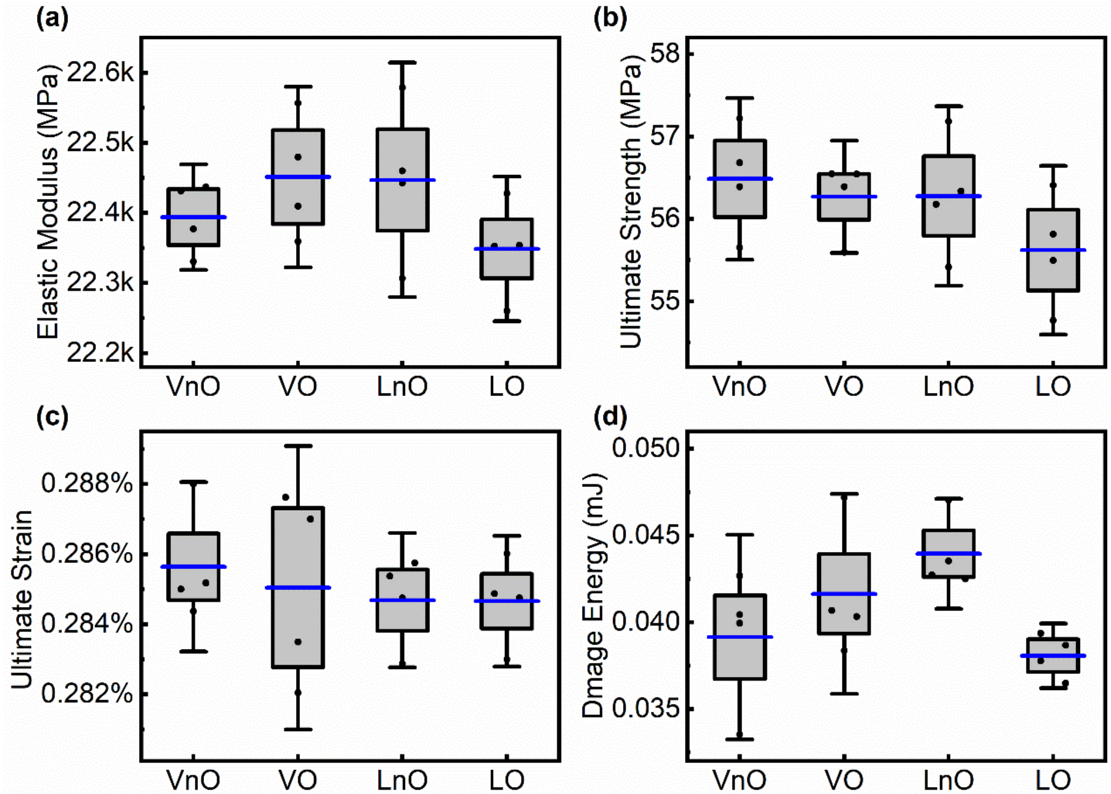

Figure 5: Groupwise comparison of mechanical properties derived from FE models. (a) Elastic modulus. (b) Ultimate strength. (c) Ultimate strain. (d) Dissipated damage energy. Error bars represent 1.5 times the standard deviation. Blue lines mark the mean values.

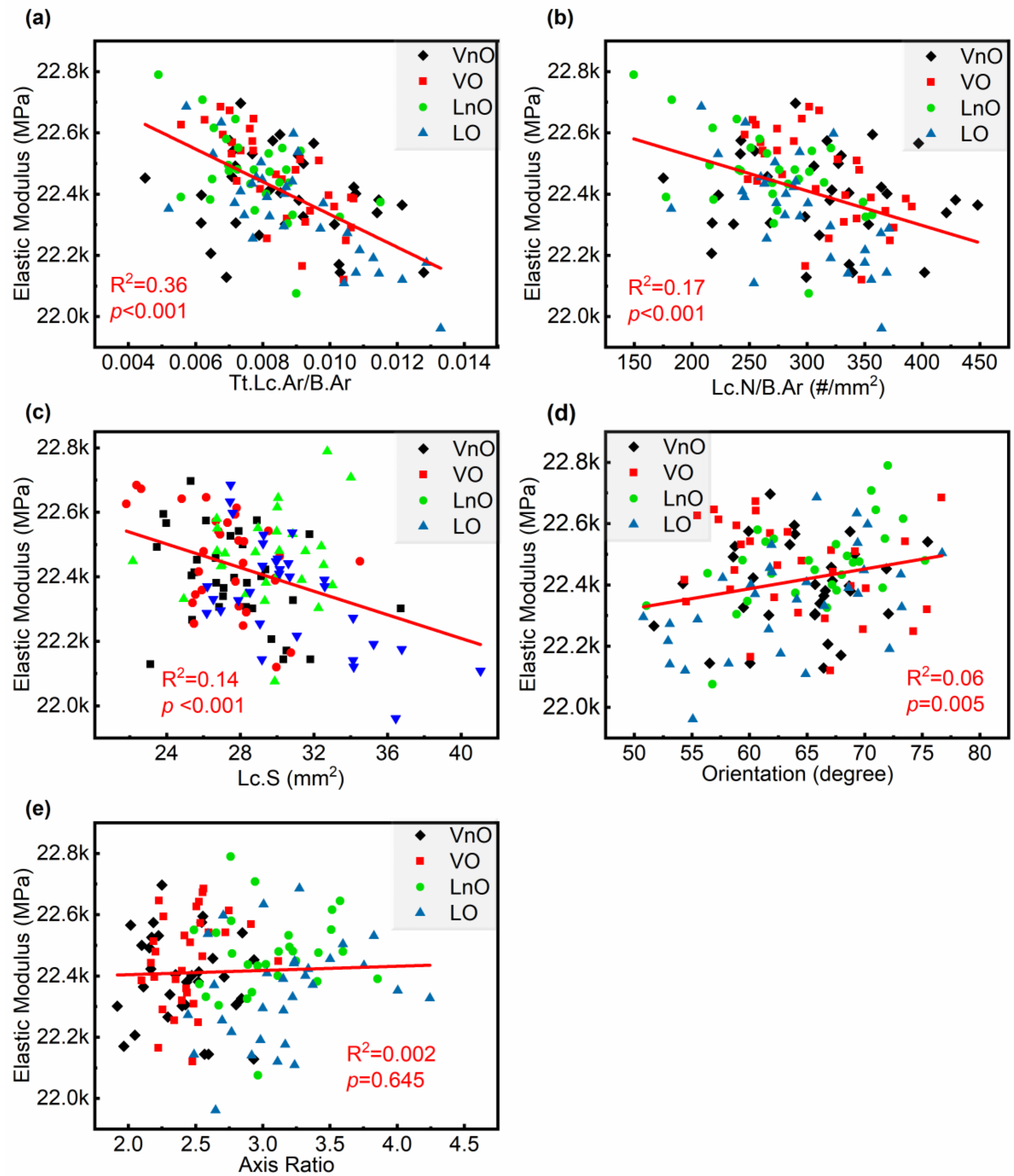

Figure 6: Variation of elastic modulus with respect to osteocyte lacunae (a) area porosity, (b) density, (c) size, (d) orientation, and (e) axis ratio and the corresponding linear regression fits.

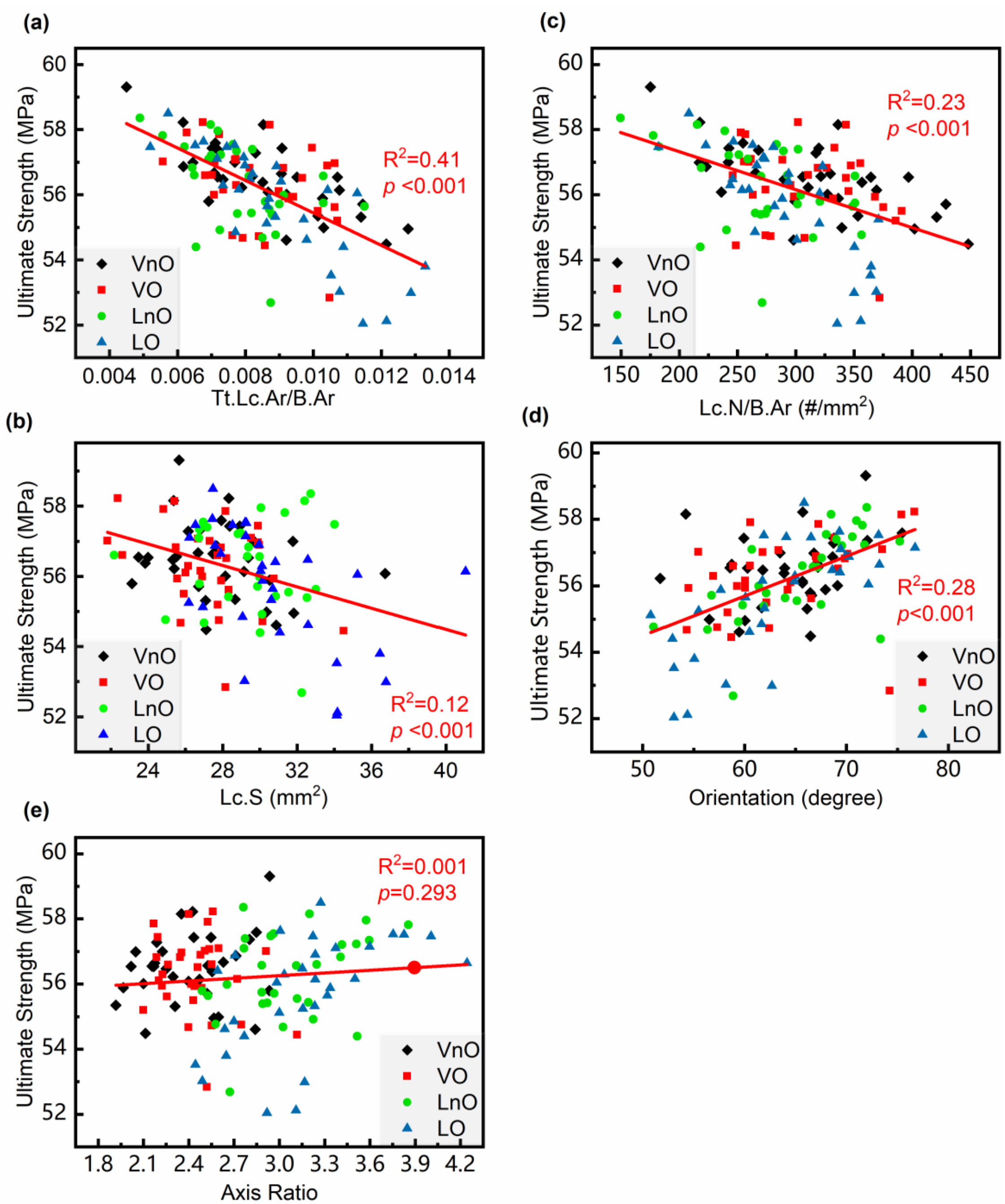

Figure 7: Variation of ultimate strength with respect to osteocyte lacunae (a) area porosity, (b) density, (c) size, (d) orientation, and (e) axis ratio and the corresponding linear regression fits.

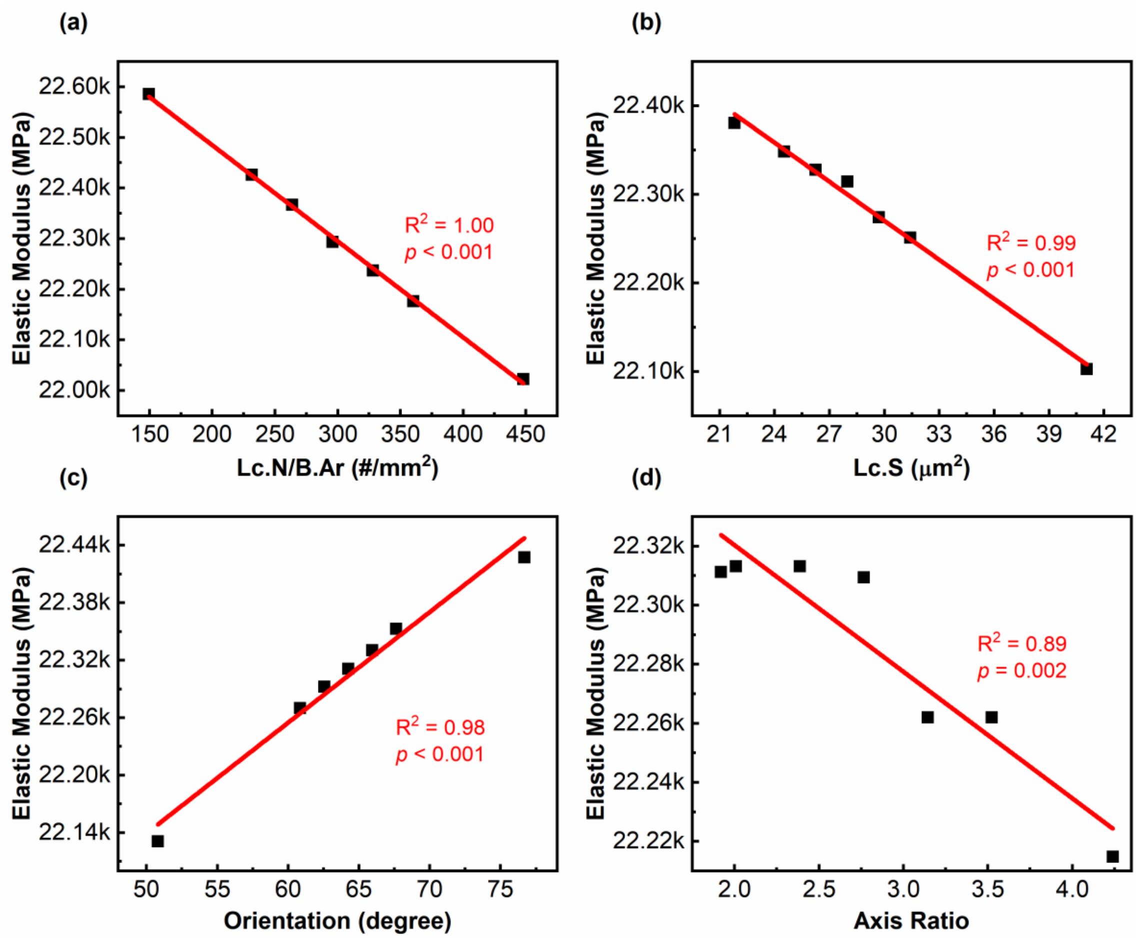

Figure 8: Variation of average elastic modulus and their corresponding linear regression fits in models where only osteocyte lacunae (a) density, (b) size, (c) orientation, and (d) axis ratio was varied.

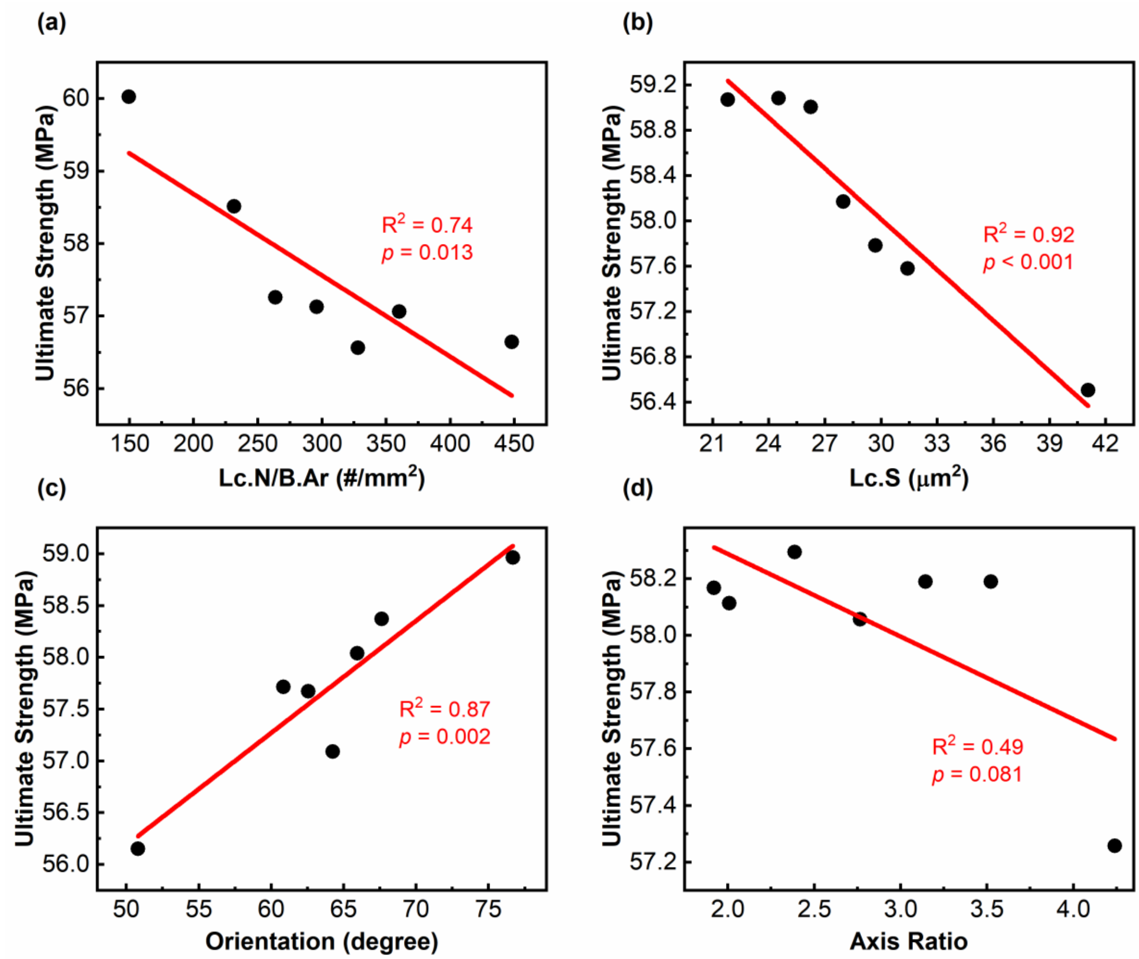

Figure 9: Variation of ultimate strength and their corresponding linear regression fits in models where only osteocyte lacunae (a) density, (b) size, (c) lacunar orientation, and (d) axis ratio was varied.

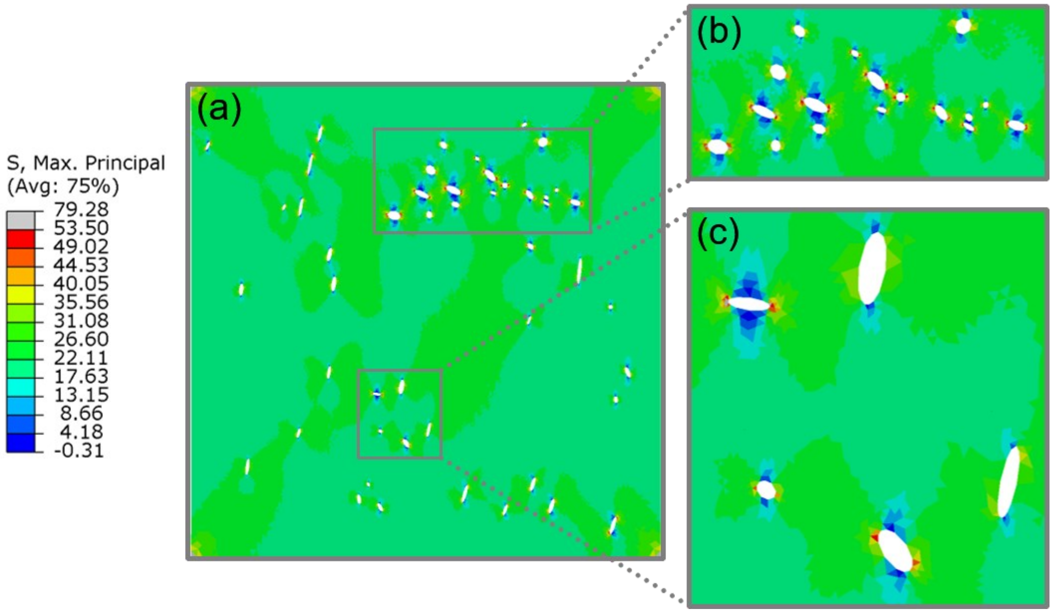

Figure 10: (a) Plot of maximum principal stress contour (in MPa) before crack initiation showing the stress concentrations near lacunar boundaries in group LnO. (b) Close-up view of stress concentrations near horizontally oriented lacunae. (c) Close-up view of stress concentrations near horizontally and vertically oriented lacunae.

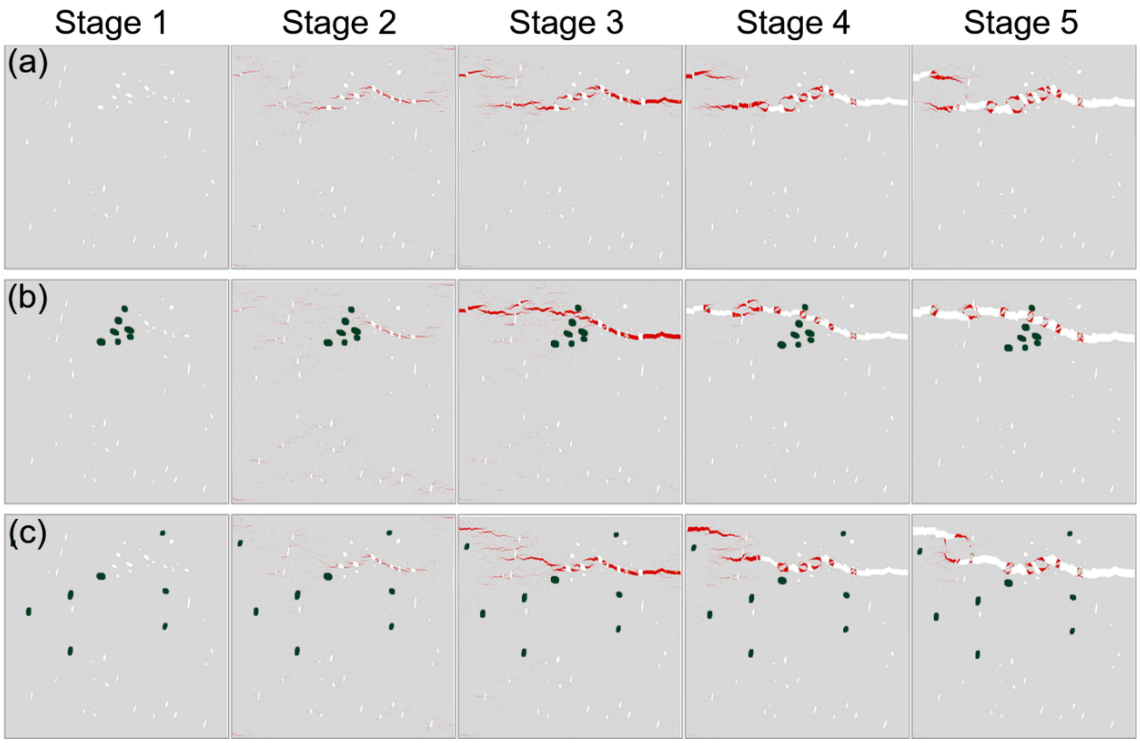

Figure 11: Representative crack propagation in the model (a) without mineralized lacuna, (b) with clustered mineralized lacunae, and (c) with scattered mineralized lacunae. Note that dark blue ellipses represent the mineralized lacunae whereas white ellipses represent the normal lacunae. Red color defines the stage at which a full crack forms. Further opening of the cracks beyond the point of full crack formation is represented by white color.

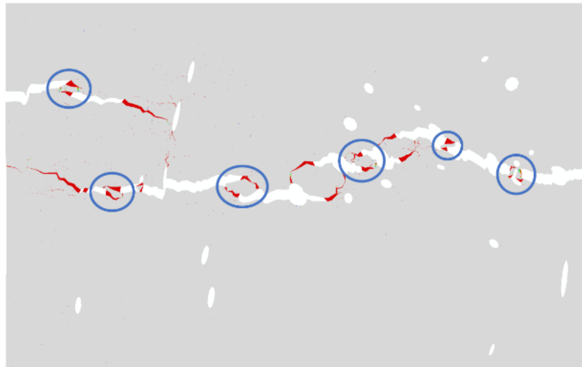

Figure 12: Snapshot of a propagating crack with multiple uncracked ligament bridging sites between adjacent osteocyte lacunae (marked by blue circle).